Quasi-Tightly-Coupled GNSS-INS Integration with a GNSS Kalman Filter

Bruno Scherzinger, *Applanix Corporation*

BIOGRAPHY

Bruno Scherzinger is the Chief Technology Officer at Applanix Corporation (a Trimble company) and an Engineering Fellow of Trimble Navigation. He is responsible for advanced navigation technology development and the core navigation technology behind the Applanix product line of Position and Orientation Systems. He has more than 30 years' experience in GNSS-INS integrated navigation systems technology, and has been a member of ION for 20 years and a member of the IEEE for 40 years. He holds 15 patents and has numerous publications in the field of geomatics and navigation.

ABSTRACT

Quasi-tightly-coupled (QTC) GNSS-INS integration is a method of loosely-coupled integration that has the salient characteristics of a tightly-coupled integration. This method is intended for the integration of an existing GNSS navigation engine into a GNSS-INS closed-loop configuration with little or no modification of the GNSS navigation engine. The method of integration uses the range measurement model matrix typically used to compute dilutions of precision (DOP) to identify the observable subspace in the time-space frame generated by the available satellites and project the loosely-coupled INS-GNSS Kalman filter position measurement into this subspace.

INTRODUCTION

Quasi-tightly-coupled (QTC) GNSS-INS integration was introduced in [1] as an enhanced method of loosely-coupled integration that has the salient characteristic of continued aiding with fewer than four satellites that a tightly-coupled integration typically exhibits. This method of integration was introduced to meet the oft-times requirement to integrate an existing and possibly sophisticated GNSS navigation engine into a GNSS-INS configuration with little or no modifications to the engine. Such a requirement might arise if the GNSS navigation engine is an RTK engine that performs well as a consequence of a sophisticated algorithm implementation, is well-tested in its commercial field of use, and is subject to tight software configuration control so that major modifications are costly and time-consuming. Another reason for considering QTC integration is the requirement for the GNSS navigation engine to operate independently of a GNSS-INS integration in case inertial data is not available or is interrupted.

The QTC integration method was presented in [1] using a simple epoch-by-epoch least squares adjustment (LSA) as the GNSS navigation engine to maintain a simple analysis while conveying the key concepts. QTC integration is however likely to be used with more sophisticated GNSS navigation engines such as a Kalman filter designed for RTK positioning. It was assumed but never shown in [1] that the same QTC integration method also applies to a Kalman filter based GNSS navigation engine. This paper removes this deficiency by presenting an analysis of the QTC integration method when the GNSS navigation engine is a Kalman filter and then by comparing the respective performances of a QTC integration and a tightly-coupled integration. In this sense this paper is a continuation of the development started in [1] .

The common attribute of a least squares adjustment and a Kalman filter is the range measurement model matrix that contains the satellite geometry. A rank deficient measurement model due to an insufficient number of satellites defines an unobservable position-time subspace in which either estimator can't produce a fully constrained position-time solution. In a tightly-coupled integration this subspace is automatically handled in the aided INS (AINS) Kalman filter. QTC integration is designed to handle such a satellite deficiency in a similar manner.

A QTC integration achieves continued aiding with fewer than four satellites using a loosely coupled AINS Kalman filter via two functional additions to a loosely coupled integration. These are *INS position seeding* of the GNSS navigation engine and an *observables subspace constraint* (OSC) in the INS-GNSS position measurement in the AINS Kalman filter. INS position seeding sets the a priori position of the GNSS navigation engine to a predicted antenna position computed from the current INS position and attitude solution. The GNSS navigation engine then computes an updated position as a correction of the a priori antenna position using the estimated position error from its GNSS Kalman filter. An unobservable dimension

in the GNSS Kalman filter solution due to insufficient satellites for full observability of position-time errors will contain uncorrected INS errors that appear in the antenna position solution sent to the AINS Kalman filter. The OCS blocks the uncorrected INS position errors from appearing in the loosely-coupled INS-GNSS position measurement constructed by the AINS Kalman filter.

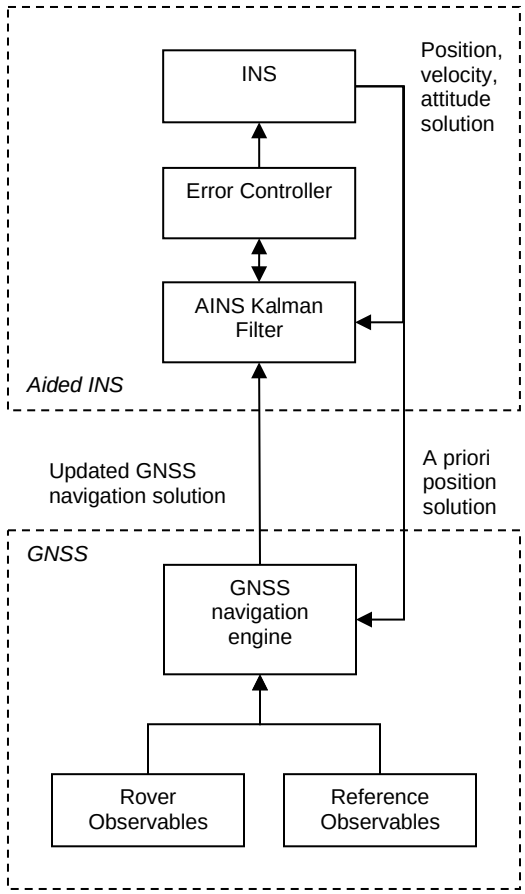

Figure 1: QTC GNSS-INS architecture

Figure 1 shows the QTC integration architecture. The one visible difference from a loosely-coupled integration is the a priori position solution from the INS to the GNSS navigation engine for implementing the INS position seeding function. Not visible is the OSC that occurs in the AINS Kalman filter's INS-GNSS position and velocity measurements.

INS POSITION SEEDING

The GNSS navigation engine in Figure 1 is a GNSS Kalman filter that processes rover receiver pseudorange observables from *m* satellites. Such a GNSS Kalman filter typically has a state vector

$$\vec{x} = \begin{bmatrix} \vec{x}_{dyn} \\ \vec{x}_{meas} \end{bmatrix} \tag{1}$$

where $\vec{x}_{dyn}$ is the state vector of a dynamics model that describes the antenna position and receiver clock error and possibly other navigation parameters such as the antenna velocity error and receiver clock drift, and $\vec{x}_{meas}$ contains the GNSS range error components such as carrier phase ambiguities, atmosphere delays and multipath errors of the different measurement models that the GNSS Kalman filter constructs. In the context of QTC integration, an elaborate vehicle dynamics model describing the antenna velocity and acceleration is redundant. INS position seeding sets the a priori antenna position to the INS predicted antenna position prior to each Kalman filter measurement update, so that the GNSS Kalman filter estimates the error in this a priori antenna position. The GNSS Kalman filter typically does not have an INS error model that describes the a priori position errors. Consequently the GNSS Kalman filter treats the a priori antenna position error as uncorrelated with the estimated position and clock error from the previous Kalman filter epoch and so throws the previously estimated position and clock error away.

For simplicity and without loss of generality, a simple GNSS Kalman filter is analyzed here in which the complete GNSS Kalman filter state $\vec{x}$ is given by

$$\vec{x} = \begin{bmatrix} \delta\vec{r}_G \\ \delta T \end{bmatrix} \tag{2}$$

where $\delta\vec{r}_G = \tilde{\vec{r}}_G - \vec{r}_G$ is the antenna position error, and δT is the receiver clock error. This is in fact the same state as was used in the LSA in [1].

The GNSS Kalman filter constructs *m* undifferenced pseudorange measurements whose measurement vector equation is given by

$$\vec{z} = H\vec{x} + \vec{\eta} \tag{3}$$

where $\vec{z}$ and H are respectively given by

and $$\vec{z} = \begin{bmatrix} \tilde{r}_1 - \rho_1 \\ \vdots \\ \tilde{r}_m - \rho_m \end{bmatrix} \qquad H = \begin{bmatrix} -\vec{u}_1^T & -1 \\ \vdots & \vdots \\ -\vec{u}_m^T & -1 \end{bmatrix} \tag{4}$$

where $\tilde{r}_i = \left|\vec{r}_i - \tilde{\vec{r}}_G\right|$ is the predicted range between satellite position $\vec{r}_i$ and the a priori antenna position $\tilde{\vec{r}}_G$, ρ_i is the GNSS range measurement for satellite *i*, $\vec{u}_i$ is the unit line of sight vector from the rover antenna to satellite *i*,

and $\vec{\eta}$ is a vector of uncorrelated Gaussian measurement noises with covariance $R = diag\begin{bmatrix} r_1 & \dots & r_m \end{bmatrix}$.

The a priori antenna position at each epoch is given by

$$\tilde{\vec{r}}_G = \tilde{\vec{r}}_{INS} = \vec{r}_{INS} + \vec{l}_{IA} \tag{5}$$

where $\vec{r}_{INS}$ is the INS position and $\vec{l}_{IA}$ is the lever arm vector from the INS position to the GNSS antenna position all resolved in an appropriate navigation coordinate frame. $\vec{l}_{IA}$ resolved in navigation frame *n* is typically computed as $\vec{l}_{IA}^{\,n} = C_b^n \vec{l}_{IA}^{\,b}$ where $\vec{l}_{IA}^{\,b}$ is the measured lever arm vector resolved in the INS body frame *b* and C_b^n is the direction cosine matrix from frame *b* to frame *n* computed from the INS roll, pitch and heading solution.

The a priori position computed from INS data comprises the true antenna position plus INS error $\delta\vec{r}_{INS}$ comprising the sum of all errors in (5).

$$\tilde{\vec{r}}_{INS} = \vec{r}_G + \delta\vec{r}_{INS} \tag{6}$$

The GNSS Kalman filter a priori state and covariance are therefore cast as follows at each epoch to reflect the unknown position and clock error that results from INS position seeding.

$$\hat{\vec{x}}^- = 0 \qquad P^- = \begin{bmatrix} P_{\delta r}^{INS} & 0 \\ 0 & P_{\delta T}^- \end{bmatrix} \tag{7}$$

The GNSS Kalman filter performs a measurement update each epoch using the following update equations.

$$\hat{\vec{x}}^+ = K\vec{z} \tag{8}$$

$$K = P^- H^T \left(HP^- H^T + R \right)^{-1} \tag{9}$$

$$\begin{aligned} P^+ &= \left(I - KH \right) P^- \\ &= P^- - P^- H^T \left(HP^- H^T + R \right)^{-1} HP^- \end{aligned} \tag{10}$$

With no state extrapolation of the estimated state between Kalman filter epochs, the observability matrix is $\mathrm{O}_n = H$ A rank deficient range measurement model *H* implies that the estimated state (2) is not observable. We use the singular value decomposition (SVD) to characterize the kernel or null space $\mathrm{Ker}(H)$ and the family of non-unique solutions [5], [6]. The SVD of an *m*×*n* matrix *H* is

$$H = U\Sigma V^T = \begin{bmatrix} U_1 & U_2 \end{bmatrix} \begin{bmatrix} \Sigma_1 & 0 \\ 0 & 0 \end{bmatrix} \begin{bmatrix} V_1^T \\ V_2^T \end{bmatrix} \tag{11}$$

where *V* is an *n*×*n* orthonormal matrix that spans the state space $\Re^n$, *U* is an *m*×*m* orthonormal matrix that spans the measurement space $\Re^m$ and Σ is an *m*×*n* trapezoidal matrix with Σ_1 a diagonal matrix of non-zero singular values. The columns of $V = \begin{bmatrix} V_1 & V_2 \end{bmatrix}$ form an orthonormal basis for $\Re^n$ in which the columns of V_2 form an orthonormal basis for $\mathrm{Ker}(H)$ the null space or kernel of *H*, and the columns of V_1 form an orthonormal basis for $\mathrm{Ker}(H)^\perp$ the orthogonal complement of the kernel of *H*. Then for any $\vec{x} \in \Re^n$ there exists $\vec{b} \in \Re^n$ such that

$$\begin{aligned} \vec{x} = V\vec{b} &= \begin{bmatrix} V_1 & V_2 \end{bmatrix} \begin{bmatrix} \vec{b}_1 \\ \vec{b}_2 \end{bmatrix} \\ &= V_1\vec{b}_1 + V_2\vec{b}_2 \\ &= \vec{x}_1 + \vec{x}_2 \end{aligned} \tag{12}$$

where $\vec{x}_1 = V_1\vec{b}_1 \in \mathrm{Ker}(H)^\perp$ and $\vec{x}_2 = V_2\vec{b}_2 \in \mathrm{Ker}(H)$. The subscripts 1 and 2 are used hereafter to indicate this subspace partition of vectors.

The estimation error vector $\vec{e} = \hat{\vec{x}} - \vec{x}$ has the following canonical representation using (12) in a basis defined by the columns of *V*.

$$\vec{e} = V\vec{e}^{\,c} = \begin{bmatrix} V_1 & V_2 \end{bmatrix} \begin{bmatrix} \tilde{\vec{e}}_1 \\ \tilde{\vec{e}}_2 \end{bmatrix} \tag{13}$$

The error covariance is cast into a corresponding canonical representation

$$P = V\mathrm{E}\left[\vec{e}^{\,c} \left(\vec{e}^{\,c} \right)^T \right] V^T = VP^cV^T \tag{14}$$

where

$$P^c = \begin{bmatrix} \mathrm{E}\left[\tilde{\vec{e}}_1 \tilde{\vec{e}}_1^T \right] & \mathrm{E}\left[\tilde{\vec{e}}_1 \tilde{\vec{e}}_2^T \right] \\ \mathrm{E}\left[\tilde{\vec{e}}_2 \tilde{\vec{e}}_1^T \right] & \mathrm{E}\left[\tilde{\vec{e}}_2 \tilde{\vec{e}}_2^T \right] \end{bmatrix} = \begin{bmatrix} P_1^c & P_{12}^c \\ P_{21}^c & P_2^c \end{bmatrix} \tag{15}$$

The components of (9) and (10) are evaluated as follows using $HV = U\Sigma V^T V = U\Sigma$.

$$HP = U\Sigma P^c V^T = \begin{bmatrix} U_1\Sigma_1 P_1^c & U_1\Sigma_1 P_{12}^c \end{bmatrix} V^T \tag{16}$$

$$PH^T = \left(HP \right)^T = V \begin{bmatrix} P_1^c \Sigma_1 U_1^T \\ P_{21}^c \Sigma_1 U_1^T \end{bmatrix} \tag{17}$$

$$HPH^T = U\Sigma P^c \Sigma^T U^T = U_1\Sigma_1 P_1^c \Sigma_1 U_1^T \tag{18}$$

The innovations covariance is given as follows for compactness.

$$\Xi = U_1 \Sigma_1 P_1^{c-} \Sigma_1 U_1^T + R \tag{19}$$

Substituting (16), (17), (18) and (19) into (10) yields the following covariance update equation.

$$\begin{aligned} P^+ &= V\left(\begin{bmatrix} P_1^{c-} & P_{12}^{c-} \\ P_{21}^{c-} & P_2^{c-} \end{bmatrix} - \begin{bmatrix} P_1^c \Sigma_1 U_1^T \\ P_{21}^c \Sigma_1 U_1^T \end{bmatrix} \Xi^{-1} \begin{bmatrix} U_1 \Sigma_1 P_1^c & U_1 \Sigma_1 P_{12}^c \end{bmatrix}\right) V^T \\ &= V\left(\begin{bmatrix} P_1^{c-} - P_1^{c-}\Sigma_1 U_1^T \Xi^{-1} U_1 \Sigma_1 P_1^{c-} & P_{12}^{c-} - P_1^{c-}\Sigma_1 U_1^T \Xi^{-1} U_1 \Sigma_1 P_{12}^{c-} \\ P_{21}^{c-} - P_{21}^{c-}\Sigma_1 U_1^T \Xi^{-1} U_1 \Sigma_1 P_1^{c-} & P_2^{c-} - P_{21}^{c-}\Sigma_1 U_1^T \Xi^{-1} U_1 \Sigma_1 P_{12}^{c-} \end{bmatrix}\right) V^T \\ &= V \begin{bmatrix} P_1^{c+} & P_{12}^{c+} \\ P_{21}^{c+} & P_2^{c+} \end{bmatrix} V^T \end{aligned} \tag{20}$$

Similarly (9) becomes the following.

$$K = V \begin{bmatrix} P_1^{c-} \Sigma_1 U_1^T \\ P_{21}^{c-} \Sigma_1 U_1^T \end{bmatrix} \Xi^{-1} \tag{21}$$

The updated estimated state (8) is characterized as follows.

$$\hat{\bar{x}}^+ = V \begin{bmatrix} \hat{\tilde{\bar{x}}}_1^+ \\ \hat{\tilde{\bar{x}}}_2^+ \end{bmatrix} = V \begin{bmatrix} P_1^{c-} \Sigma_1 U_1^T \Xi^{-1} \bar{z} \\ P_{21}^{c-} \Sigma_1 U_1^T \Xi^{-1} \bar{z} \end{bmatrix} \tag{22}$$

Equations (20) and (22) show that the estimated state and covariance can be separated into the following observable and unobservable components in a basis defined by the columns of *V*.

$$\begin{aligned} \hat{\tilde{\bar{x}}}_1^+ &= P_1^{c-} \Sigma_1 U_1^T \Xi^{-1} \bar{z} \\ P_1^{c+} &= P_1^{c-} - P_1^{c-} \Sigma_1 U_1^T \Xi^{-1} U_1 \Sigma_1 P_1^{c-} \end{aligned} \tag{23}$$

$$\begin{aligned} \hat{\tilde{\bar{x}}}_2^+ &= P_{21}^{c-} \Sigma_1 U_1^T \Xi^{-1} \bar{z} \\ P_2^{c+} &= P_2^{c-} - P_{21}^{c-} \Sigma_1 U_1^T \Xi^{-1} U_1 \Sigma_1 P_{12}^{c-} \end{aligned} \tag{24}$$

The updated state in the original basis is

$$\begin{aligned} \hat{\bar{x}}^+ &= \hat{\bar{x}}_1^+ + \hat{\bar{x}}_2^+ \\ &= V_1 \hat{\tilde{\bar{x}}}_1^+ + V_2 \hat{\tilde{\bar{x}}}_2^+ \end{aligned} \tag{25}$$

and its covariance is given by (20).

P_{21}^{c-} is characterized as follows after a measurement update from an initial state (7). $VP^c = PV$ contains

$$\begin{bmatrix} V_1 P_1^c + V_2 P_{21}^c & V_1 P_{12}^c + V_2 P_2^c \end{bmatrix} = \begin{bmatrix} PV_1 & PV_2 \end{bmatrix} \tag{26}$$

and hence

$$P_{21}^c = V_2^T P V_1 - V_2^T V_1 P_1^c = V_2^T P V_1 \tag{27}$$

This shows that $P_{21}^{c-} = 0$ is equivalent to the columns of $P^- V_1$ being in $\mathrm{Ker}(H)^\perp$. An example where this happens is $P^- = \sigma^2 I$. In this case $\hat{\tilde{\bar{x}}}_2^+ = 0$ and $\hat{\bar{x}}^+ = V_1 \hat{\tilde{\bar{x}}}_1^+$. This is in general not the case as can be shown with almost any $P^- = \mathrm{diag}\begin{bmatrix} p_1 & \cdots & p_m \end{bmatrix}$ having unequal diagonal elements. The GNSS Kalman filter update

$$\begin{aligned} \hat{\bar{x}}_2^+ &= V_2 \hat{\tilde{\bar{x}}}_2^+ \\ &= V_2 P_{21}^{c-} \Sigma_1 U_1^T \Xi^{-1} \bar{z} \end{aligned} \tag{28}$$

of the unobservable sub-state is therefore sensitive to the a priori cross-covariance P_{21}^{c-} between observable and unobservable states. Typically the a priori covariance P^- is a diagonal matrix assembled from limited information and therefore does not contain a model of the cross-correlations between states. $\hat{\bar{x}}_2^+$ is therefore an unreliable estimate of $\bar{x}_2$ that should be removed before the estimated state is used to compute a GNSS position solution. This can be accomplished by filtering the estimated state as follows to block $\hat{\tilde{\bar{x}}}_2^+$ before it is used to correct the a priori GNSS position.

$$\begin{aligned} V_1 V_1^T \hat{\bar{x}}^+ &= V_1 V_1^T \left(V_1 \hat{\tilde{\bar{x}}}_1^+ + V_2 \hat{\tilde{\bar{x}}}_2^+ \right) \\ &= V_1 \hat{\tilde{\bar{x}}}_1^+ = \hat{\bar{x}}_1^+ \end{aligned} \tag{29}$$

The resulting estimate now resembles the LSA estimate described in [1].

OBSERVABLE SUBSPACE CONSTRAINT

The estimated position error from the estimated state (22) is used to compute the corrected GNSS position as $\hat{\bar{r}}_G = \tilde{\bar{r}}_G - \delta \hat{\bar{r}}_G^+$ from the a priori position $\tilde{\bar{r}}_G$ given by (5) where $\delta \hat{\bar{r}}_G^+$ is obtained from (25) with

$$\hat{\bar{x}}_1^+ = \begin{bmatrix} \delta \hat{\bar{r}}_{G1}^+ \\ \delta \hat{T}_1^+ \end{bmatrix} \text{ and } \hat{\bar{x}}_2^+ = \begin{bmatrix} \delta \hat{\bar{r}}_{G2}^+ \\ \delta \hat{T}_2^+ \end{bmatrix} \tag{30}$$

In a normal loosely-coupled integration, the AINS Kalman filter constructs a three dimensional loosely-

coupled INS-GNSS position measurement comprising the difference between the INS position and the updated GNSS position. The AINS Kalman filter typically assumes the following measurement model in which INS and GNSS position errors $\delta\bar{r}_{INS}$ and $\delta\tilde{\bar{r}}_G$ are uncorrelated

$$\begin{aligned}\bar{z}_{IG} &= \tilde{\bar{r}}_{INS} - \hat{\bar{r}}_G = \delta\bar{r}_{INS} - \delta\tilde{\bar{r}}_G \\ &= A\bar{x}_{AINS} + \bar{\eta}_{IG}\end{aligned} \tag{31}$$

where A is the AINS Kalman filter measurement model matrix and $\bar{\eta}_{IG}$ is the uncorrelated measurement noise model. Without INS position seeding, the assumed measurement model (31) is fairly reliable.

If $m < 4$ and INS position seeding is used, the AINS Kalman filter measurement is in fact the following.

$$\bar{z}_{IG} = \delta\bar{r}_{INS1} - \delta\hat{\bar{r}}^{+}_{G1} + \delta\bar{r}_{INS2} - \delta\hat{\bar{r}}^{+}_{G2} \tag{32}$$

$\delta\hat{\bar{r}}^{+}_{G2}$ is an unreliable estimate of $\delta\bar{r}_{INS2}$ and may in fact be zero as was the case when $P^{-} = \sigma^2 I$. In either case the IG measurement and its measurement model in the AINS Kalman filter are inconsistent as described by the assumed (31) and actual (32) measurement models. This inconsistency results in AINS Kalman filter biases and can cause the AINS error regulation loop in Figure 1 to become unstable.

The inconsistency is resolved by using the observable subspace constraint (OSC) matrix $\Gamma = V_{d1}^T$ described in [1] that has the property $\Gamma\Delta\delta\bar{r}_{INS2} = 0$, so that the constrained measurement model correctly describes the constrained measurement.

$$\begin{aligned}\Gamma\bar{z}_{IG} &= \Gamma\left(A\bar{x}_{AINS} + \bar{\eta}_{IG}\right) \\ &= \Gamma\left(\delta\bar{r}_{INS1} - \delta\tilde{\bar{r}}_{G1}\right)\end{aligned} \tag{33}$$

The construction of the OSC matrix from [1] is reviewed here as follows. The following non-singular transformation matrix implements a single-difference operation on m satellites observables to construct m-1 satellite differenced measurements

$$D = I - B$$

$$B = \begin{bmatrix} 0_{m-1\times m-1} & \bar{b} \\ \hline & 0_{1\times m} \end{bmatrix} \quad \bar{b} = \begin{bmatrix} 1 \\ \vdots \\ 1 \end{bmatrix}_{1\times m-1} \tag{34}$$

(34) applied to (3) and (4) gives a transformed measurement model $\bar{z}_D = H_D\bar{x} + \bar{\eta}_D$ where

$$\bar{z}_D = D\bar{z} = \begin{bmatrix} \bar{z}_d \\ \hat{r}_m - \rho_m \end{bmatrix} \tag{35}$$

$$H_D = DH = \begin{bmatrix} H_d & 0 \\ -\bar{u}_m^T & -1 \end{bmatrix} \tag{36}$$

$$\bar{z}_d = \begin{bmatrix} \Delta\hat{r}_1 - \Delta\rho_1 \\ \vdots \\ \Delta\hat{r}_{m-1} - \Delta\rho_{m-1} \end{bmatrix} \quad H_d = \begin{bmatrix} -\Delta\bar{u}_1^T \\ \vdots \\ -\Delta\bar{u}_{m-1}^T \end{bmatrix} \tag{37}$$

where $\Delta\bar{u}_i^T = \bar{u}_i^T - \bar{u}_m^T$ for i=1,…,m-1.

The *Kernel Equivalence Lemma* from [1] shows that

$$\begin{bmatrix} \delta\bar{r} \\ \delta T \end{bmatrix} \in \mathrm{Ker}\left(H\right)$$

is equivalent to $\delta\bar{r} \in \mathrm{Ker}\left(H_d\right)$ and $\bar{u}_m^T\delta\bar{r} = -\delta T$.

The SVD (11) applied to H_d yields matrices V_{d1} and V_{d2} that respectively span $\mathrm{Ker}\left(H_d\right)^{\perp}$ and $\mathrm{Ker}\left(H_d\right)$. This implies that $V_{d1}^T\bar{x}_{d2} = 0$ for any $\bar{x}_{d2} \in \mathrm{Ker}\left(H_d\right)$. The Kernel Equivalence Lemma applied to (32) shows that

$$\delta\bar{r}_{INS2} - \delta\hat{\bar{r}}^{+}_{G2} \in \mathrm{Ker}\left(H_d\right) \tag{38}$$

and hence the OSC matrix from [1] fulfills the requirement for (33) to hold.

$$V_{d1}^T\left(\delta\bar{r}_{INS2} - \delta\hat{\bar{r}}^{+}_{G2}\right) = 0 \tag{39}$$

SIMULATION EXPERIMENT

The QTC integration method has been tested extensively using simulation experiments, such as described here, and actual navigation missions. The following experiment taken from [1] used data recorded by an Applanix POS AV during an airborne survey mission whose horizontal trajectory is shown in Figure 2. The POS AV contained a tactical grade (1-10 degrees/hour gyro bias) IMU and a dual frequency GPS receiver. A dual frequency GPS reference receiver was set up at the airport at which the mission started and ended. The purpose of the experiment was to evaluate the position errors generated by each of the following three AINS mechanizations through partial GPS outages. The first AINS mechanization contained a sophisticated and high-performance RTK engine in a standard loosely coupled configuration. The second AINS mechanization comprised the first mechanization with

QTC integration as shown in Figure 1. The third AINS mechanization comprised a tightly-coupled inertially aided RTK integration as described in [2] and [3].

60-second partial outages to 3 satellite were simulated in the recorded rover receiver data as shown in Figure 3. The reference trajectory for the experiments was a smoothed best estimate of trajectory (SBET) generated by Applanix's POSPac post-mission software.

Figure 4 show the North position error with a loosely coupled non-QTC integration. The RTK engine is unable to recover from outages occurring when the aircraft is farthest from the airport and the baseline length becomes large (on the order of 50 kilometers). Figure 5 shows the North position error with QTC integration. Figure 6 shows the North position error generated by a tightly-coupled integration with inertially aided RTK described in [2] and [3] and implemented by Applanix's POSPac post-mission software. Both the QTC integration and tightly-coupled integration yielded comparable position error growths during the simulated partial satellite outages. These plots show that QTC integration generates smaller position error growths during the partial outages and faster recoveries of RTK position accuracies when the outages end than does a standard loosely-coupled non-QTC integration.

Interestingly the QTC integration yielded somewhat better performance than the tightly coupled integration. This outcome is a consequence of the better performance of the state-of-the-art RTK engine used in the QTC integration when compared with the more dated kinematic ambiguity resolution algorithm in the version of POSPac that was used in this experiment. It shows that a true comparison of QTC and tightly-coupled integrations requires both integration methods to implement the same GNSS processing and kinematic ambiguity resolution algorithms (which was beyond the scope of this experiment).

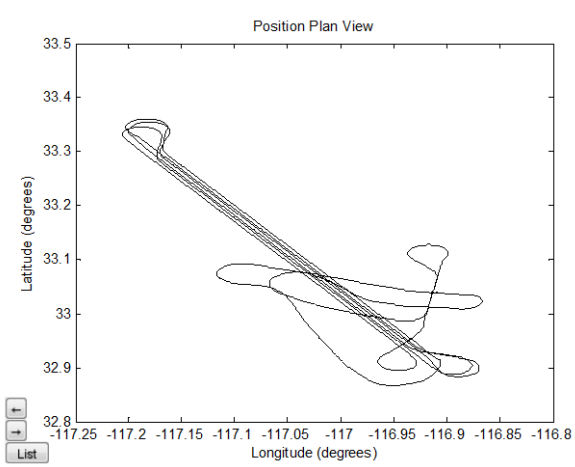

Figure 2: Airborne survey trajectory

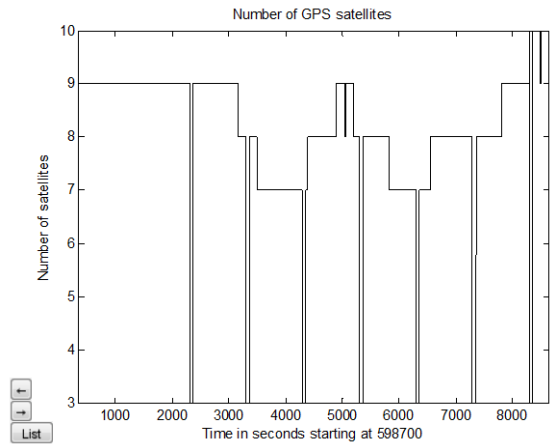

Figure 3: Visible GPS satellites

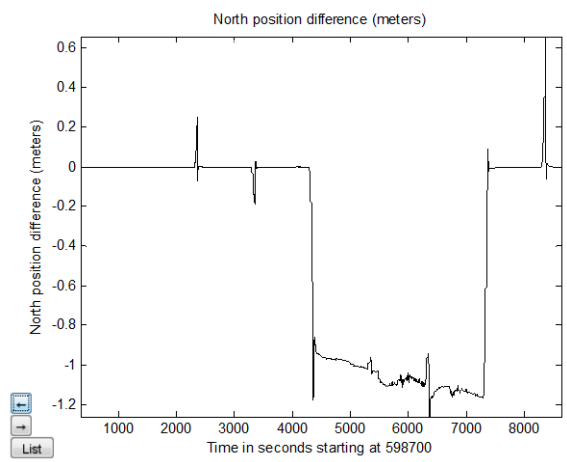

Figure 4: North position error without QTC integration

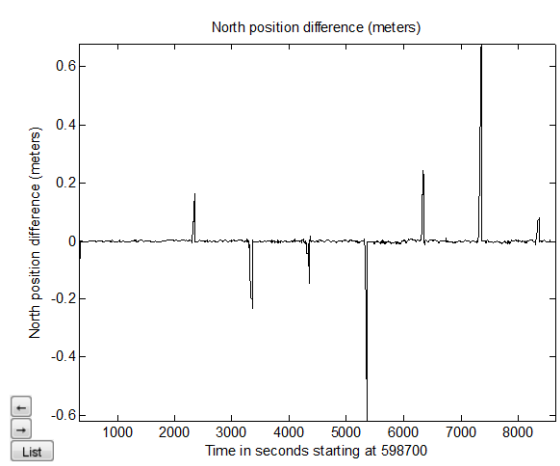

Figure 5: North position error with QTC integration

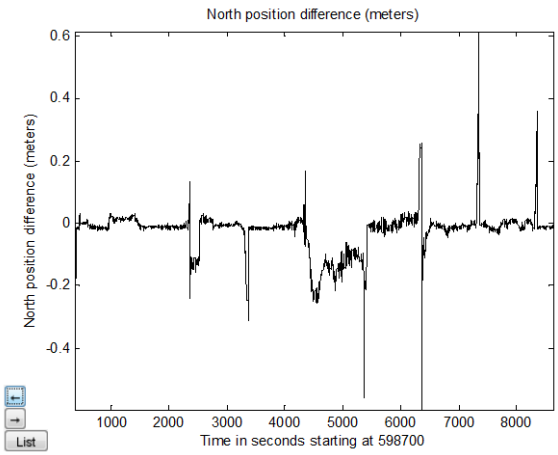

Figure 6: North position error from a tightly coupled integration

CONCLUSIONS

This paper has expanded on [1] by demonstrating how the QTC integration method works with a GNSS navigation engine that is a Kalman filter. QTC integration adds INS position seeding to the GNSS Kalman filter and an observable subspace constraint to the AINS Kalman filter's INS-GNSS position measurement in order to obtain tightly-coupled behavior from the loosely-coupled integration. INS seeding allows the GNSS Kalman filter to estimate the a priori antenna position errors in the observable subspace with fewer than four satellites. The resulting estimated position error contains an unreliable and possible zero antenna position error estimate in the unobservable position-time subspace defined by the deficient satellite geometry. This is the same limitation on position-time error observability and estimation as in a tightly-coupled integration. The same OSC that was used in [1] in a QTC integration of a least squares adjustment is also used here in a QTC integration of a GNSS Kalman filter. The OSC constrains the INS-GNSS position measurement construction to the observable position-time subspace and thereby avoids erroneous modeling of the INS position error in the AINS Kalman filter.

This paper has expanded on some experimental results from [1] to demonstrate the effectiveness of QTC integration. The partial outage experiment showed that QTC integration provided lower position drift and faster RTK recovery than a loosely-coupled integration is capable of. This paper has added some experimental results on the comparative performances of tightly-coupled and QTC integrations. The literature is replete with articles on the superior performance of a tightly-coupled integration over a loosely coupled integration. The expectation is that a QTC integration will in general perform better than a loosely-coupled integration but not as well as a tightly-coupled integration. This paper has shown an example in which a QTC integration has benefited from a particularly good GNSS navigation engine having fast and reliable RTK positioning capability that is not easily built into a tightly-coupled integration. In such a case a QTC integration can outperform a tightly-coupled integration.

The QTC integration method described in this paper is the subject of a patent [7].

REFERENCES

[1] Scherzinger, B., Quasi-Tightly-Coupled GNSS-INS Integration, Proceedings of ION GNSS+ 2014, Tampa FL, September 2014.

[2] Scherzinger, B., Precise Robust Positioning with Inertial/GPS RTK , Proceedings of ION GPS 2000, Salt Lake City UH, September 2000.

[3] Scherzinger, Bruno M., Precise Robust Positioning with Inertially Aided RTK, NAVIGATION, Journal of The Institute of Navigation, Vol. 53, No. 2, Summer 2006, pp. 73-84.

[4] Applied Optimal Estimation 12th Edition, Arthur Gelb (editor), MIT Press 1992.

[5] Numerical Recipes in C++, The Art of Scientific Computing – Second Edition, Cambridge University Press, 2002.

[6] Gander, Walter, The Singular Value Decomposition, ETH Zurich, December 12, 2008.

[7] US 8825396 B2 Quasi-Tightly-Coupled GNSS-INS Integration Process, filing date 30 November 2012, publication date 30 September 2014.